Cold Air Mass Analysis of the Record-Breaking Cold Surge Event over East Asia in January 2016

Junpei YAMAGUCHI

Department of Geophysics, Graduate School of Science, Tohoku University, Sendai, Japan

Yuki KANNO

Institute for Space-Earth Environmental Research, Nagoya University, Nagoya, Japan
Geophysical Institute, University of Bergen, Bergen, Norway
Bjerknes Centre for Climate Research, Bergen, Norway

Guixing CHEN

Center for Monsoon and Environment Research, School of Atmospheric Sciences, Sun Yat-sen University, China
Guangdong Province Key Laboratory for Climate Change and Natural Disaster Studies, Sun Yat-sen University, China

and

Toshiki IWASAKI

Department of Geophysics, Graduate School of Science, Tohoku University, Sendai, Japan

(Manuscript received 21 March 2018, in final form 6 November 2018)

Abstract

An extreme cold surge event caused record-breaking low temperatures in East Asia during 20–25 January 2016. The planetary- and synoptic-scale feature of the event is investigated quantitatively using the isentropic cold air mass analysis with a threshold potential temperature of 280 K. Because cold air mass is an adiabatically conservative quantity, it is suitable for tracing and examining the extreme cold surges. We further introduced a metric named mean wind of cold air mass, which divides the factor of cold air mass evolution into convergence and advection parts. The new metric allowed us to trace the evolution of the cold air mass with dynamic consistency for a period of more than a week.

A thick cold air mass built up over southern Sakha by a convergent cold air mass flow during 16–18 January. It migrated westward and reached Lake Baikal. On 20 January, an intense Siberian High developed, with an eastward-moving mid-upper-level ridge, producing a strong surface pressure gradient over the coastal regions of the Asian continent. This ridge and a cutoff low to the adjacent east formed a northerly flow in the mid-upper troposphere. The resultant southward flow through the troposphere blew the cold air mass over 480 hPa in thickness to the subtropical region of East Asia, causing strong cold surges there on 24 and 25 January.

The abnormality of the event is further quantified using extreme value theory. The cold air mass gradually became rare along the path of the cold air mass from Lake Baikal to eastern China, which experienced as thick

Corresponding author: Junpei Yamaguchi, Department of Geophysics, Graduate School of Science, Tohoku University, A519, Physics A Building, 6-3, Aoba, Aramaki, Aoba-ku, Sendai 980-8578, Japan
E-mail: junpeiy@dc.tohoku.ac.jp
J-stage Advance Published Date: 24 November 2018

a cold air mass as once in 200 years. The cold air mass itself shows little change in thickness. Therefore, the migration of a cold air mass over 540 hPa in thickness from northern Siberia is the major cause of this cold surge extreme.

Keywords cold air outbreak; cold air mass; cold surge; East Asian winter monsoon; extreme low temperature

Citation Yamaguchi, J., Y. Kanno, G. Chen, and T. Iwasaki, 2019: Cold air mass analysis of the record-breaking cold surge event over East Asia in January 2016. *J. Meteor. Soc. Japan*, **97**, 275–293, doi:10.2151/jmsj.2019-015.

1. Introduction

The East Asian winter monsoon (EAWM), a dominant circulation system in the northern hemisphere during boreal winter, strongly affects the weather and climate of East Asian countries (Ding and Sikka 2006). In fact, the EAWM is characterized by a strong Siberian High (SH), an Aleutian low, and a strong pressure gradient between them, with resultant strong northerly or northwesterly winds at the surface (Zhang et al. 1997; Chang et al. 2006; Wang and Lu 2016). The activity of the EAWM shows various behaviors in a wide range of timescales such as intra-seasonal and interannual variation. The strong EAWM is often related with the invasion of cold and dry air, which causes accelerated northerlies and abrupt temperature drops throughout East Asia (Ding and Krishnamurti 1987; Ding and Sikka 2006; Wang and Lu 2016). Such events, called cold air outbreaks (CAOs), are often associated with the southeastward expansion of the intensified SH (Ding and Krishnamurti 1987). Accompanying the CAO, cold air blows over continental East Asia, sometimes reaching the South China Sea in a short period (Chang et al. 1983; Zhang et al. 1997). This outburst of cold air (i.e., cold surge) shows prevailing northeasterly movement near the surface and below 700 hPa (Ding 1990; Ding and Sikka 2006).

Intra-seasonal variations of the SH and EAWM are closely related to the middle- and upper-tropospheric circulation patterns. Some reports have described a relation among the EAWM activities, CAO occurrence, and the upper tropospheric wave-like patterns which propagate downstream across the Eurasian continent (Joung and Hitchman 1982; Zhang et al. 1997; Park et al. 2014). Takaya and Nakamura (2005a) examined the "Wave-train (Atlantic-origin) type" circulation, which corresponds to a Eurasian (EU)-like pattern modulated by a planetary wave (Wallace and Gutzler 1981; Wang and Lu 2016). They found that the interaction between low-level cold anticyclonic anomaly and the upper-level wave train plays an important role in the dramatic intensification of both anomalies, which results in CAOs. Some other studies have demonstrated that the formation of atmospheric blocking on the subarctic region can modulate EAWM and engender CAO (e.g., Park et al. 2014). Takaya and Nakamura (2005b) suggested that in the "Pacific origin type" circulation pattern, which is similar to the Western Pacific (WP) teleconnection pattern (Wallace and Gutzler 1981), the blocking ridge over the north of the Sea of Okhotsk advects background cold air to the north of the Tibetan Plateau and brings CAO through a similar vertical interaction as the wave-train (Atlantic-origin) type.

Intense cold surges sometimes cause societal effects in the form of strong winds, extreme low temperatures, and subsequent freezing rain or heavy snowfall (Ding and Krishnamurti 1987). The extreme cold surge events in January 2016 in East Asia have drawn considerable attention in both public and research communities. On 24 January 2016, snowfall was observed for the first time in 115 years at Amami-Oshima (refer to the sites in Fig. 1), Japan. Sleet fell in Okinawa prefecture, which had not recorded sleet since 1977. Rare snowfall/graupel was even observed in Guangzhou, the largest city of southern China. China National Climate Center (2017) reported that most areas of mainland China experienced a dramatic temperature drop during 20–25 January 2016, with record-breaking low temperatures at 69 sites. Taipei recorded its lowest temperatures in 43 years, and the minimum temperatures in Hong Kong dropped to 3.1°C, the lowest in 59 years. Many weather organizations and researchers had focus on the large-scale processes associated with this extreme CAO event (e.g., Oikawa and Kamiguchi 2016). Cheung et al. (2016) pointed out that strengthening of the stratospheric Aleutian anticyclone and blocking in the Ural region and North America jointly cause a split of the polar vortex and an abrupt phase reversal of the Arctic Oscillation (AO) index, which orients the circulation patterns more meridionally and is favorable for the

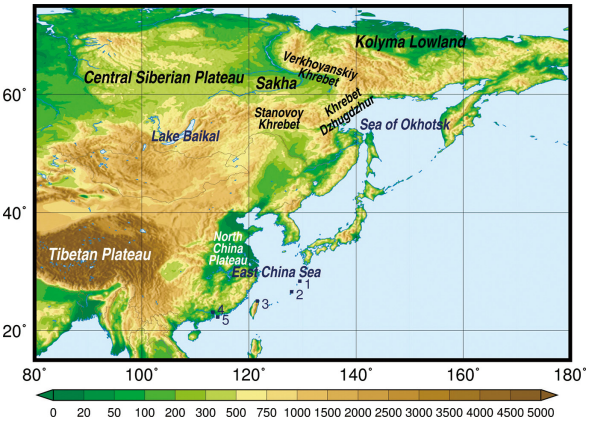

Fig. 1. Map of eastern Asia. Shading shows topography (m). Words are names of places mentioned in text. Five map points represent these locations: (1) Amami-Oshima, (2) Okinawa, (3) Taipei, (4) Guangzhou, and (5) Hong Kong.

occurrence of CAO. To date, most earlier studies have elucidated the cause of cold surges from synoptic circulation or in terms of external large-scale forcing. Nevertheless, quantitative analysis of the cold air mass itself is currently unavailable for such extreme events.

To monitor the intensity and variation of cold surges readily and quantitatively, Iwasaki et al. (2014; referred to as I14 hereinafter) proposed a method of isentropic analysis that defines a cold air mass as an air mass below a threshold potential temperature. The method allows for a quantitative diagnosis of cold air and cold surges as cold air masses, which are generated by diabatic cooling alone. Without the diabatic process, cold air masses move as a conserved variable. The I14 study revealed two clear climatological cold air mass streams by isentropic analysis of cold air mass flux: East Asian and North American cold streams. The East Asian cold stream grows over the northern part of the Eurasian continent, flows eastward, turns southeastward around Siberia, and disappears over the western North Pacific Ocean. Shoji et al. (2014) defined several indices to reproduce East Asian CAO as outflowing southward flux of cold air mass across 45°N. For instance, their western CAO index, which is defined by the integrated southward flux between 90°E and 135°E, corresponds to the developing SH and transient Okhotsk low. Abdillah et al. (2017) showed that the western CAO is correlated well with positive EU, negative WP, and negative AO patterns in an interannual timescale and that it is related with La Niña-like events. Kanno et al. (2015) analyzed the polar cold air mass and CAO using a two-box model of cold air mass, which comprises a genesis box north of 45°N and a loss box south of 45°N. They found that after CAO, the increased cold air mass amount in the loss box is taken away only in a few days. The isentropic cold air mass analysis is also applied to case studies. For example, Papritz and Pfahl (2016) applied this method to the CAO in Ross, Amundsen, and Bellingshausen Seas. They found the importance of mesocyclones for the decay of CAO, which cause fragmentation of CAO and incursion of warmer air, and for the role of latent heat release accompanying sensible heating as an agent effecting CAO erosion.

To date, understanding of the dynamical linkage between CAO and synoptic or large-scale circulations in a view of isentropic cold air mass remains insufficient, especially for the extreme events of CAO that cause record-breaking low temperatures and rare snowfall in East Asia. A recent study showed that, during the extreme event in January 2016, the intensity of the East Asian cold stream is the strongest since the winter of 1981/1982 (Oikawa and Kamiguchi 2016). In the present paper, we further apply the isentropic cold air mass framework of I14 to investigate this extreme CAO event. We specifically examine the origin, development, and path of the cold surge as well as its relation to large-scale circulations.

This paper is organized as follows. Section 2 introduces the data and analysis methods used for this study. Section 3 presents the circulation field associated with the extreme CAO event of January 2016. In Section 4, we investigate this CAO event using the isentropic cold air mass framework. The cold surge is described as a flow of thick cold air mass. We also investigate the formation processes, migration route, and decay stage of the cold air mass. Section 5 presents visualization of the rarity of the CAO event. In Section 6, we discuss the relation among the evolution of cold air mass, the synoptic or large-scale mid-to-lower level circulation field, and upper-level circulations. A summary of findings is presented in Section 7.

2. Data and methods

2.1 Data source

For this study, we use the Japanese 55-year Reanalysis (JRA-55) with a spatial resolution of 1.25° latitude × 1.25° longitude at 37 pressure levels (1000 to 1 hPa) with an interval of 6 hour (Kobayashi et al. 2015). The climatological mean, standard deviation, and other statistics are based on the 6-hourly data in

winter time (December to February) of the 50-year period of 1966/1967–2015/2016. In addition to analytical fields, we use a 6 hour forecast-mean heating rate due to long-wave radiative, convective, large-scale condensation and vertical diffusion heating. We did not use the short-wave radiative heating rate because of negligible contribution.

2.2 Cold air mass analysis

To analyze the cold surge event, we use the formulas of cold air mass analysis derived in I14. The cold air mass is defined as a pressure difference between the geographical surface and the isentropic surface of the threshold potential temperature θ_T as

$$DP \equiv p_s - p(\theta_T), \tag{1}$$

where p_s signifies the surface pressure and $p(\theta_T)$ denotes the pressure on isentrope $\theta = \theta_T$. This definition denotes the cold air mass thickness with a potential temperature below θ_T when the hydrostatic equilibrium condition is satisfied and when no static unstable layer exists. We set $\theta_T = 280$ K as in I14. The cold air mass flux is defined using horizontal wind $\mathbf{v}$ as shown below

$$\mathbf{F} \equiv \int_{p(\theta_T)}^{p_s} \mathbf{v} dp. \tag{2}$$

The formula of the time variation of the cold air mass (1) can be written as

$$\frac{\partial}{\partial t} DP = -\nabla \cdot \mathbf{F} + \frac{\partial p}{\partial \theta} \dot{\theta}\Big|_{\theta_T}, \tag{3}$$

where $\dot{\theta}$ denotes the total derivative of the potential temperature, which corresponds to diabatic heating. The first term on the right-hand side represents the cold air mass rate of change because of the convergence of the cold air mass flux (2), and the second term stands for the effect of diabatic heating/cooling at θ_T isentrope.

Combining (1) and (2), we may define a mean wind of the cold air mass:

$$\mathbf{v}_\mathrm{m} \equiv \mathbf{F} \cdot DP^{-1}. \tag{4}$$

The benefit of such a vector is to divide the cold air mass flux (2) into two components that are contributed, respectively, by the amount of cold air mass and by the wind field. Using this definition, we can rewrite the formula of the time variation of the cold air mass (3) as shown below

$$\frac{\partial}{\partial t} DP = -(\mathbf{v}_\mathrm{m} \cdot \nabla) DP - DP(\nabla \cdot \mathbf{v}_\mathrm{m}) + \frac{\partial p}{\partial \theta} \dot{\theta}\Big|_{\theta_T}. \tag{5}$$

The convergence of the cold air mass flux in (3) (the first term on the right-hand side) is divided into the first two terms on the right-hand side of (5). The first term denotes the advection of the cold air mass by the mean wind of the cold air mass. The second term denotes the convergence of the mean wind of the cold air mass that might reflect a build-up of cold air mass by convergence when positive. In a limit of shallow cold air mass, which means that air below $\theta = \theta_T$ is confined to the ground surface and has very shallow thickness, $\mathbf{v}_\mathrm{m}$ converges to a wind at the level of $p = p_s$. Therefore, we define $\mathbf{v}_\mathrm{m}$ as the surface velocity (10 m velocity of the JRA-55 dataset) on the region where DP is zero. This definition causes a difference only on the $DP = +0$ contours in the time variation of the cold air mass. Therefore, we omit the description of the mean wind where the cold air mass is zero, except in Section 5, where we treat the mean wind as the measure of the intensity of the wind which blows the cold air mass.

To include the information of coldness, we use the negative heat content as in I14:

$$\vartheta \equiv \int_{p(\theta_T)}^{p_s} (\theta_T - \theta) dp. \tag{6}$$

The negative heat content flux is given as shown below

$$\mathbf{NHF} \equiv \int_{p(\theta_T)}^{p_s} (\theta_T - \theta) \mathbf{v} dp. \tag{7}$$

The relation between the negative heat content and its flux is written as follows:

$$\frac{\partial}{\partial t} \vartheta = -\nabla \cdot \mathbf{NHF} - \int_{p(\theta_T)}^{p_s} \dot{\theta} dp. \tag{8}$$

The first term on the right-hand side shows the negative heat content rate of change attributable to the convergence of the negative heat content fluxes. The second term on the right-hand side represents a diabatic effect, which is the sum of diabatic heating/cooling from the surface to θ_T isentrope.

In our analysis, except Section 4.3, the diabatic generation/loss terms of the cold air mass (the last term of (3)) and negative heat content (the last term of (8)) are calculated conversely using (3) and (8), respectively, using a time derivative of the cold air mass and convergence of its fluxes. In Section 4.3, cold air mass tendencies due to several diabatic effects are

calculated directly by the respective heating rate listed in Section 2.1.

2.3 Extreme value analysis

To quantify the abnormality of the CAO event that struck East Asia on 24 January 2016, we evaluate the return periods of the respective values using generalized extreme value (GEV) distribution. The cumulative frequency function of GEV is a function having three parameters and might be written as follows:

$$F(x;\mu,\beta,\xi)=\exp\left\{-\left[1+\xi\left(\frac{x-\mu}{\beta}\right)\right]^{-1/\xi}\right\}. \quad (9)$$

We first take the annual maximum values from the period of 1967–2016. Such data consisting of the maxima in a certain period are called the block maxima data. According to the theory of extreme value, the distribution of block maxima data can be approximated with GEV distribution in appropriate conditions (e.g., Takahashi and Shimura 2016).

In our study, package "ismev" (e.g., Stephenson 2018) of open-source software R (http://www.r-project.org/) is used to fit the data to GEV distributions. We first apply the maximum likelihood method to obtain three parameters of cumulative frequency functions in each grid point using 50 annual maxima of the respective grid point. Then, we use the cumulative density function to calculate the return period of the maximum value in this event.

3. Synoptic features of the record-breaking CAO event in January 2016

First, we briefly introduce the synoptic atmospheric field associated with the CAO. Figure 2a shows the sea-level pressure and its anomaly at 00UTC during 16–24 January, 2016. On 16 January, the SH is located on the Central Siberian Plateau (around 65°N, 100°E; refer to Fig. 1 for the name of places). During 16–20 January, the center of the SH propagates westward and southward. On 22 January, the SH reaches a maximum pressure higher than 1060 hPa; its anomaly exceeds twice the climate-mean standard deviation. Afterward, the SH propagates southward to southern China and the South China Sea, where many regions experience abnormally high pressure of more than three times the standard deviation. On 24 January, low pressure has developed over Japan. Between the SH and the low pressure, a strong pressure gradient is formed near the coast of the East Asian continent.

Figure 2b presents the evolution of 500-hPa geopotential height and its anomaly during the same period as that shown in Fig. 2a. On 16 January, an intense ridge occupies the arctic region of Siberia (marked with "R1") and lies slightly north of the surface SH. In the subarctic region at approximately 50°N, two cutoff cyclones are recognizable: one over the Sea of Okhotsk ("T1") and the other over northeastern Mongolia ("T2"). The former moves westward, and the latter propagates eastward; they merge with each other on 18 January. The two cutoff lows proceed, respectively, westward and eastward. On 20 January, "T1" comes to Lake Baikal, and "T2" goes to the east coast of northern Japan. During 18–20 January, another mid-level ridge ("R2") propagates from Middle East to western Siberia. "R1" is merged with "R2" on 20 January, becoming indistinguishable from the propagating ridge (and marked with "R" hereafter). On 22 January, "T1" propagates southward to eastern Mongolia. "R" has a northeast–southwestward oriented axis and a large extent of anomalous high geopotential height exceeding twice the standard derivation. On 24 January, "T1" moves southeastward and forms a deep trough over the East China Sea. Northwestward of it is "R" with a winding anomaly pattern. Cheung et al. (2016) pointed out that this lower-tropospheric and upper-tropospheric circulation pattern on 22 January is favorable for the formation of extremely strong SH, which is also noted for other cold events (Takaya and Nakamura 2005a; Wang et al. 2010; Cheung et al. 2013). Cheung et al. (2016) also described that the blocking due to "R1" on 16 January occurred simultaneously when the AO attains the peak of its negative phase.

4. Quantifying cold air mass associated with the record-breaking CAO event

4.1 Evolution of the cold air mass

To provide further insight into the event, the evolution of the CAO in terms of cold air mass and cold air mass flux is depicted in Fig. 3. At 00UTC 16 January, a thick cold air mass exists over the Sea of Okhotsk (marked with "C1"), with its depth exceeding 540 hPa. A thin cold air mass is located at Kolyma Lowland ("C2"). On 18 January, the thick cold air mass is established at southern Sakha ("C"), which is surrounded by mountains: Stanovoy Khrebet (mountain range; see Fig. 1), Khrebet Dzhugdzhur, and Verkhoyanskiy Khrebet. Over "C" and on the northern side of "C1", a westward and northwestward cold air mass flux is dominant. To the southeast of "C1", a strong southeastward cold air mass flux exists. These two fluxes of opposite directions elongate and sprit "C1". During 18–20 January, "C" migrates west-

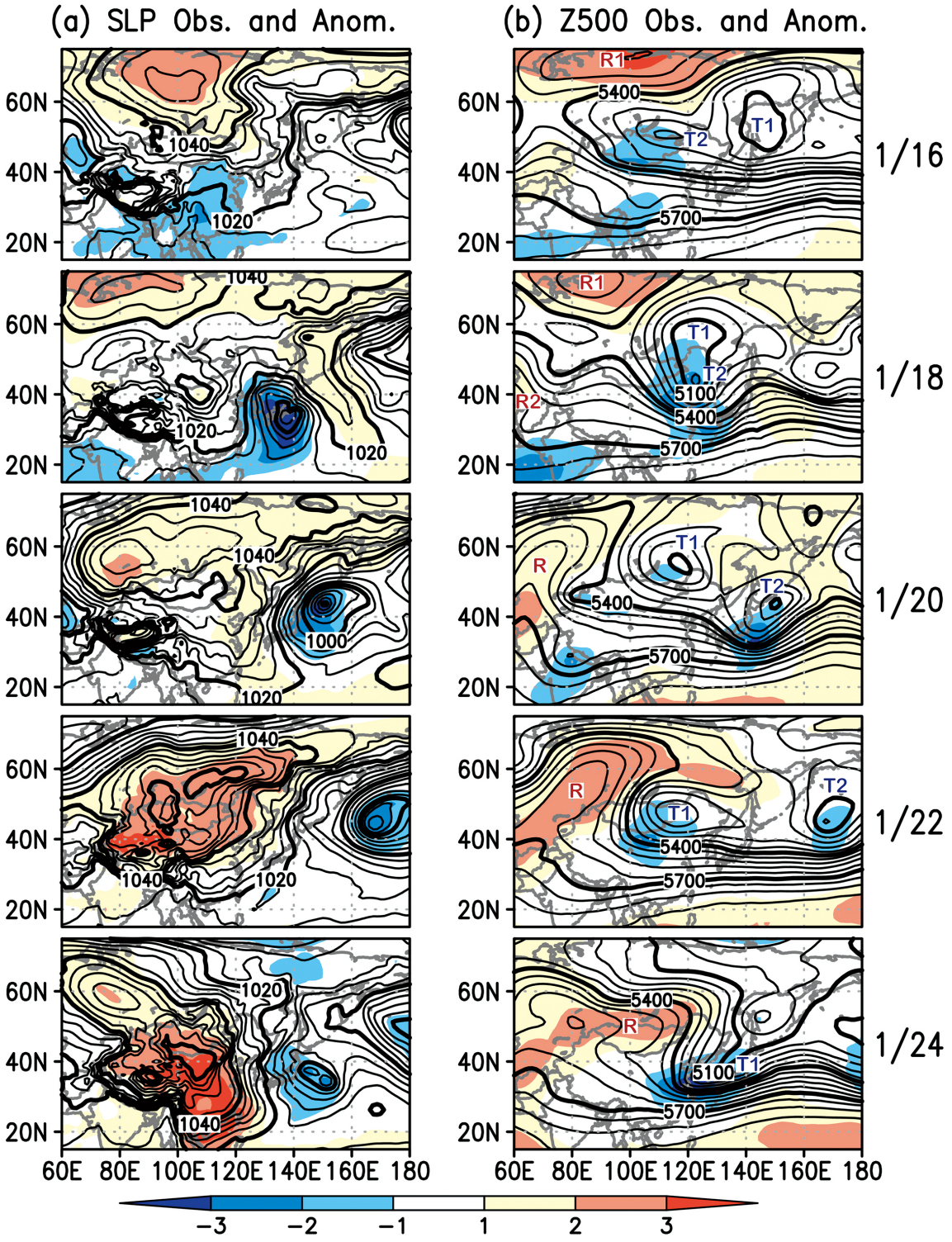

Fig. 2. Time series of (a) pressure reduced to mean sea level and (b) geopotential height on 500 hPa during 16–24 January 2016 at 00UTC. Contours show observed values. Shading shows its anomaly normalized by standard deviation. The contour interval is 4 hPa in (a) and 60 m in (b). Every fifth contour is bold. The labels "R" specify ridges, and "T1" and "T2" specify troughs.

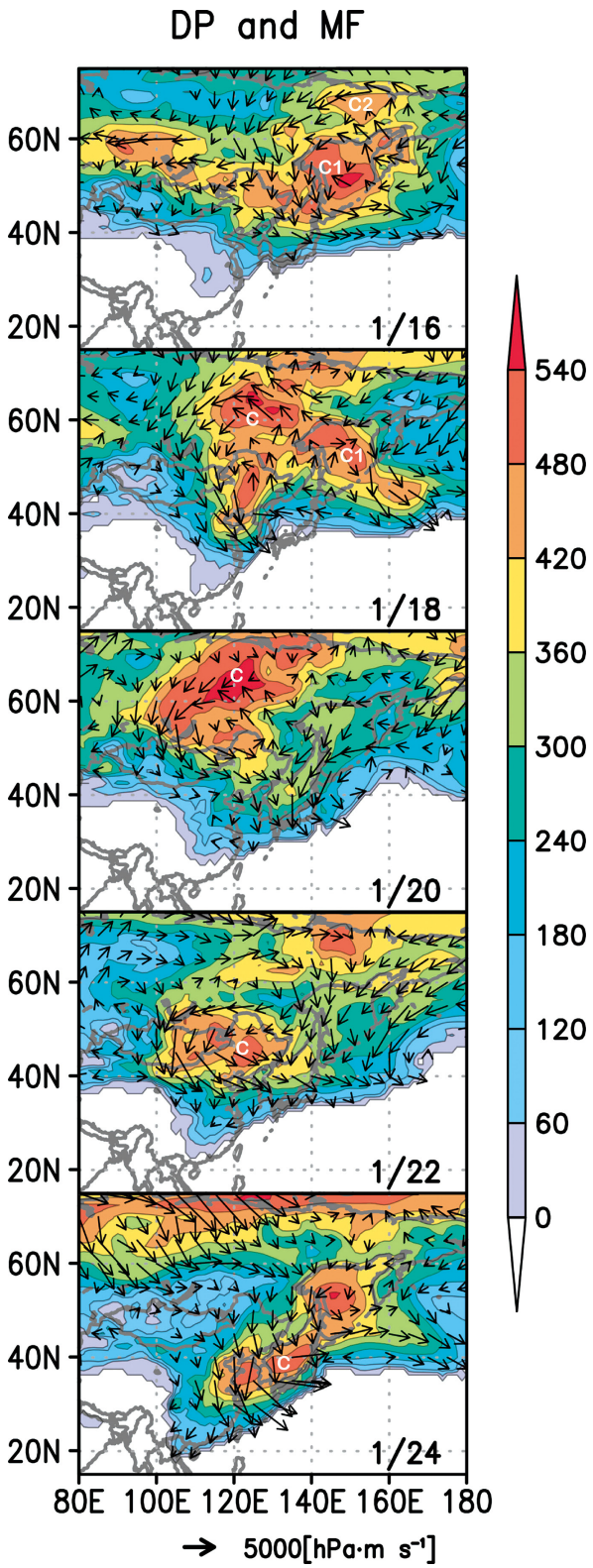

ward along the Stanovoy Khrebet, reaching northeast of Lake Baikal with a maximum depth above 540 hPa over the Central Siberian Plateau. After reaching Lake Baikal, "C" undergoes a sudden change in its migration route from west to south on 20 January. On 22 January, "C" moves southward and is located on northeastern China. On 24 January, the center of "C" is located on the Sea of Japan. The edge of the cold air mass reaches farther to the south of Japan and southern China, including Amami-Oshima, Okinawa, Taipei, Guangzhou, and Hong Kong.

To investigate the cause of change in the distribution of the cold air mass, we show the 2-day mean tendency of the cold air mass and its contribution from respective mechanisms in Fig. 4. Figure 4a shows the cold air mass mean tendency. The positive cold air mass tendency region related to the earlier described thick cold air mass "C" is enclosed by circles: near southern Sakha during 16–18 January and north of Lake Baikal during 18–20 January. During 20–22 January, it is located around Mongolia. The cold air mass rate of change has a dipole pattern during 22–24 January: the positive tendency is located in eastern China, and a negative one is on the north of it near Lake Baikal. Figure 4b shows the mean cold air mass change rate due to cold air mass flux convergence, or adiabatic dynamical mechanisms. Its spatial pattern mostly coincides with the full rate of change of the cold air mass. By contrast, the diabatic generation rate of the cold air mass in Fig. 4c generally has a positive tendency over the continent. The negative tendency attributable to diabatic heating occurs mainly over the ocean surface, especially on the edge of the cold air mass.

Both adiabatic and diabatic mechanisms contribute to the cold air mass positive tendency related with "C" over the continent. To evaluate the relative importance of both mechanisms, we calculate the areal average of those terms over the grid box moving with the thick cold air mass. To do this, we first estimate the position of the "center of the cold air mass" using that of local maxima. We note that the local maximum thickness of the cold air mass displays some discontinuity in 6-hourly diagrams because of the influence of the

Fig. 3. Cold air mass (hPa; shaded) and cold air mass flux (hPa m s^{-1}; arrows) during 16–24 January 2016 at 00UTC. The labels "C1", "C2", and "C" represent the cold air masses referred in the text.

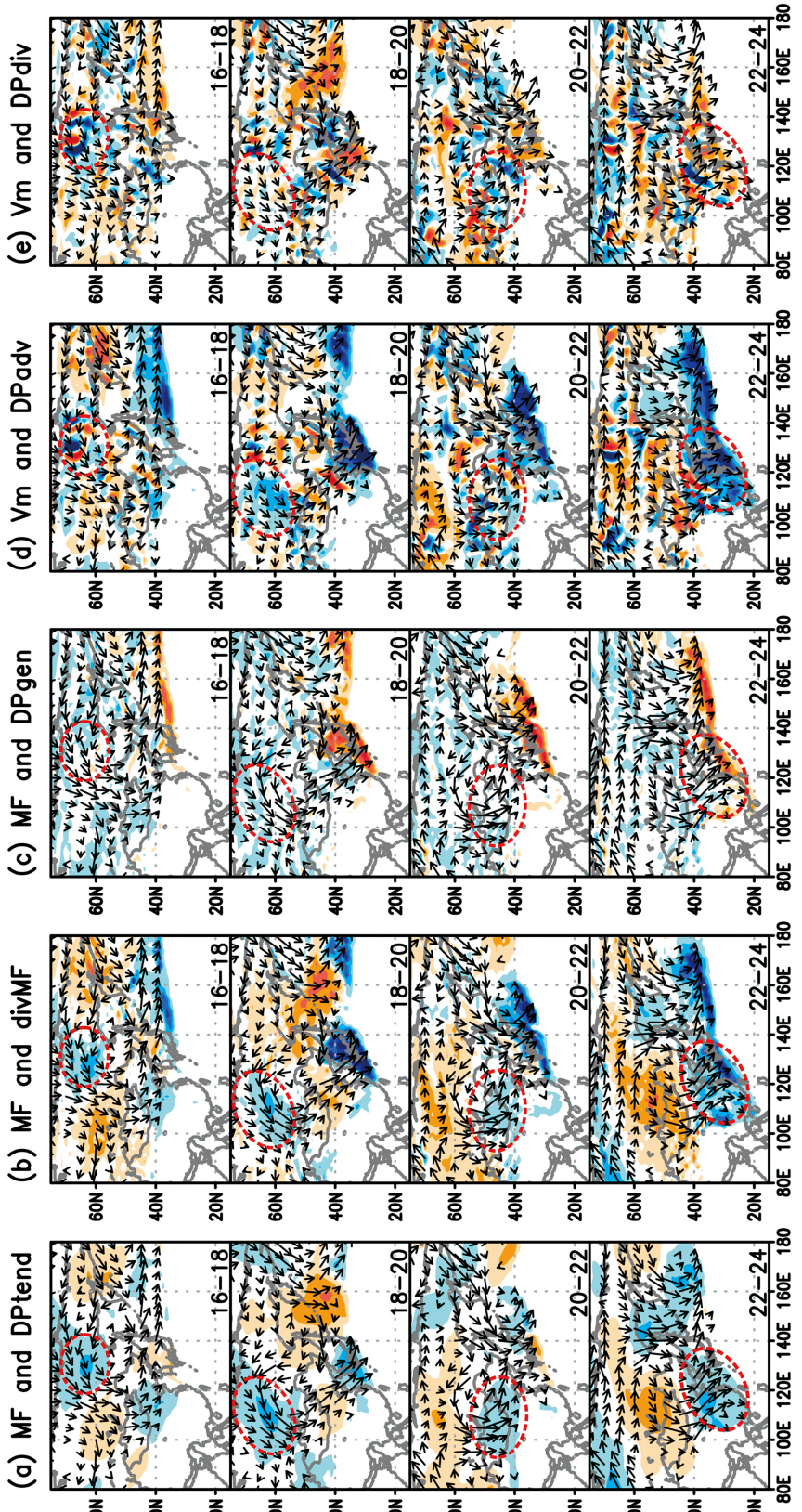

Fig. 4. Two-day average of (a) cold air mass tendency and contribution to it associated with (b) cold air mass flux convergence (hPa day^{-1}; shaded) (the first term on the right-hand side of (3)), (c) cold air mass diabatic genesis/loss rate (hPa day^{-1}; shaded) (the last term of (3)), (d) advection of cold air mass by mean wind (hPa day^{-1}; shaded), and (e) convergence of mean wind (hPa day^{-1}). The averaging period is written at the bottom-right side of figures: from 00UTC of the first day to 00UTC of the last day in January 2016. Arrows indicate the averaged cold air mass flux (hPa m s^{-1}) in (a–c) and the mean wind (m s^{-1}) in (d–e). The region enclosed by circles represents the cold air mass developing region referred in the text.

terrain (figure not shown). To represent the inherent smooth movement of the air mass, here we estimate its 6-hourly track based on relatively precise positions at six specific days using cubic interpolation as shown in Fig. 5b. Second, we define the moving grid box such that its center coincides with the "center of the cold air mass" at the time, with its size about 1110 km along the meridian and parallel over the center. Some of them are shown in Fig. 5b. Next, we define the value of the tendency term as the averaged value of its snapshot from two days before, intending to detect why the center is located there. For instance, the value on 18 January here is, in fact, the averaged value during 16–18 January. Finally, the moving-grid-box mean tendency term is calculated by averaging the value over the box. The result is shown in Fig. 5a. From the figure, we can see that the cold air mass change rate is always positive in the analyzed period. Around 18–19 January and after 22 January, the adiabatic contribution exceeds 50 hPa day^{-1} and becomes dominant. The diabatic contribution, on the other hand, is relatively constant and always positive before 06UTC 23 January and becomes negative when the cold air mass reaches the ocean region. Comparing two contributions, the value of adiabatic contribution is twice or larger than that of diabatic contribution most of the period. Consequently, the migrating cold air mass on the Asian continent as depicted in Fig. 3 is caused mostly by the adiabatic dynamical processes, whereas diabatic generation plays a secondary role in the intensification or maintenance of the cold air mass.

Comparing the cold air mass and its flux in Fig. 3 to the synoptic pattern in Fig. 2, we note some relations between the two distributions. First, the thick cold air mass is collocated with the mid-level cutoff cyclone portrayed in Fig. 2b. During 16–20 January, the direction of the cold air mass flux over the thick cold air mass "C2" on Kolyma Lowland and "C" on southern Sakha is consistent with the geostrophic wind between the cutoff cyclone and a ridge on the arctic region. This is also the case of the cold air mass flux over the west side of the thick cold air mass on 22 January. The cutoff cyclone and propagating ridge northwest of it make a strong height gradient where the strong southward to southeastward fluxes exist. It is also shown that sea-level pressure contours are dense over there. Considering the features described above, the thick cold air mass seems to be closely related with the large-scale or synoptic-scale atmospheric fields.

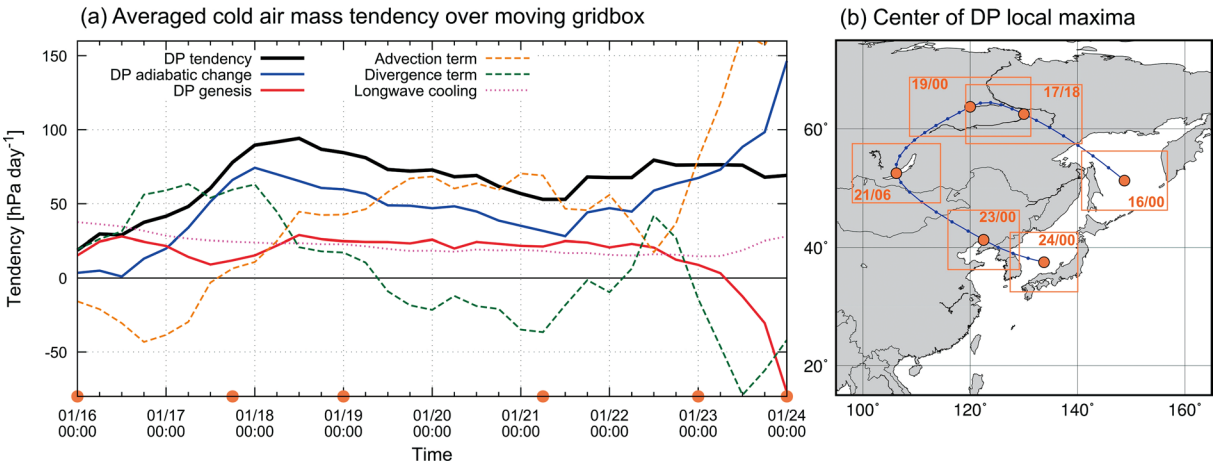

Fig. 5. (a) Time series of areal averaged cold air mass tendency (black, bold) and contribution to it associated with cold air mass flux convergence (blue), cold air mass diabatic generation rate (red), advection of cold air mass by mean wind (orange, dashed), convergence of mean wind (green, dashed), and long-wave radiative cooling (pink, dotted). The averaging area is inside the box enclosed by the meridian and parallel whose center coincides with that of the cold air mass, which is shown as orange and blue points in Fig. 5b. Its size is about 1110 km along the meridian and parallel over the center. Tendency terms are calculated by averaging the values for two days, the end of which is the day denoted in the x axis. (b) Simplified trajectory of cold air mass. Orange points represent the position of the local maxima of the cold air mass on the time denoted by the orange text, and enclosing rectangles are the shape of the boxes. Blue curve and points are a path and the 6-hourly positions of the cold air mass estimated by connecting the orange circles using cubic spline.

4.2 Advection and divergence of cold air mass

Considering that the adiabatic dynamical process plays a primary role, we further investigate the dynamical mechanisms evolving the cold air mass using the newly introduced mean wind and tendency equation of (5). Figure 4d shows the time-averaged mean wind of the cold air mass and the rate of change of the cold air mass attributable to advection by the mean wind, i.e., the first term on the right-hand-side of (5). The positive rate of change of the cold air mass because of advection related to the thick air mass is collocated well with the rate of change because of the flux convergence of the cold air mass during 18–22 January (c.f. Figs. 4b, d). For that reason, the cold air mass migrates much like a moving clump during the period, with a little change because of its gathering or creation. This can be also confirmed by Fig. 5a: the positive tendency of cold air mass adiabatic change is mostly because of the advection term in the period. During 22–24 January, the increase of the cold air mass caused by cold air mass advection is stronger than that caused by the convergence of cold air mass fluxes (Figs. 4d, 5a). The advection term has two peaks on 22 January: one on the Yellow Sea and Japan and the other on the south of the North China Plateau and reaching southern China. Many earlier reports have described that the cold surge tends to take the route along the eastern edge of the Tibetan Plateau (e.g., Zhang et al. 1997). Therefore, the peak on the south of the North China Plateau corresponds with the preferred path of the cold surge along the topography.

Figure 4e presents the contribution of cold air mass convergence by the mean wind to the cold air mass change rate. At 00UTC 16 January, convergence is observed on southern Sakha. Around that region, strong northerly and northeasterly winds exist, which correspond to the cold air mass flux over the northwest side of the cold air mass on the Kolyma Lowland, indicating that the cold air mass flowed from Kolyma Lowland converging to southern Sakha. Some strong divergence of the mean wind is apparent over the northwestern Pacific and southern Sea of Okhotsk during 18–20 January, the center of which is located around 42°N, 155°E. This region is where "C2" is located; therefore, strong divergence represents spitting of "C2". The mean wind blows northward and westward, in general, over the western and northern parts of the region to push the cold air mass to the adjacent continent. As shown in Fig. 5a, the convergence of the mean wind explains well the positive tendency of the cold air mass before 00UTC 18 January. But after that, it makes at most a weak contribution to cold air mass development, and strengthening divergence begins after 06UTC 19 January to diminish cold air mass clump "C". During 22–24 January, large-scale strong divergence regions are located on the coastal region of China and the East China Sea (Fig. 4e). A large part of the region is the same as that of the region of cold air mass increase caused by advection. Consequently, two processes are mutually offset there.

4.3 Factors contributing to cold air mass diabatic genesis and loss

We saw that diabatic generation is widespread over the continent, but the loss of the cold air mass has a much narrower distribution over the ocean. As inferred from the study of Boville (1985), Ding and Krishnamurti (1987), and Ding (1990), the diabatic generation of cold air mass is presumed to be because of radiative cooling. Figure 5a also represents the cold air mass change rate attributable to long-wave radiative cooling. Before 23 January, cold air mass adiabatic generation is almost explainable by the contribution from radiative cooling. Note that the contribution from radiative cooling is always positive even over the ocean. Therefore, it indicates that other dominant contributors to cold air mass loss exist over the ocean.

I14 suggests that the sharpness of the loss region is attributable to the warm ocean current at the western boundary of the Pacific. To detect what diabatic processes cause the negative tendency over the ocean, Fig. 6 presents the time average of cold air mass generation/loss rate during 22/12–27/00 UTC and its contribution from vertical diffusion heating and the sum of convective and large-scale condensation heating. Heating due to vertical diffusion affects more at the edge of the cold air mass probably because the cold air mass erodes when the sensible heat flux reaches 280 K isentrope. Surface upward sensible heat fluxes are strongly positive over the ocean where the cold air mass is located (not shown), and vertical diffusion may be the transporter of the flux. Therefore, what restricts the area of erosion is a reach of the flux, and the thin layer of the cold air mass is needed for erosion. By contrast, precipitation-related heating is widespread on the sea around Japan, which Papritz and Pfahl (2016) pointed out as an important factor for cold air mass erosion. When averaging in the box (120–140°E, 20–40°N) shown in Fig. 6, the mean loss rates of the cold air mass by vertical diffusion heating and precipitation-related heating are 29.2 and 27.6 hPa day^{-1}, respectively. Therefore, both processes equally contribute to cold air mass erosion.

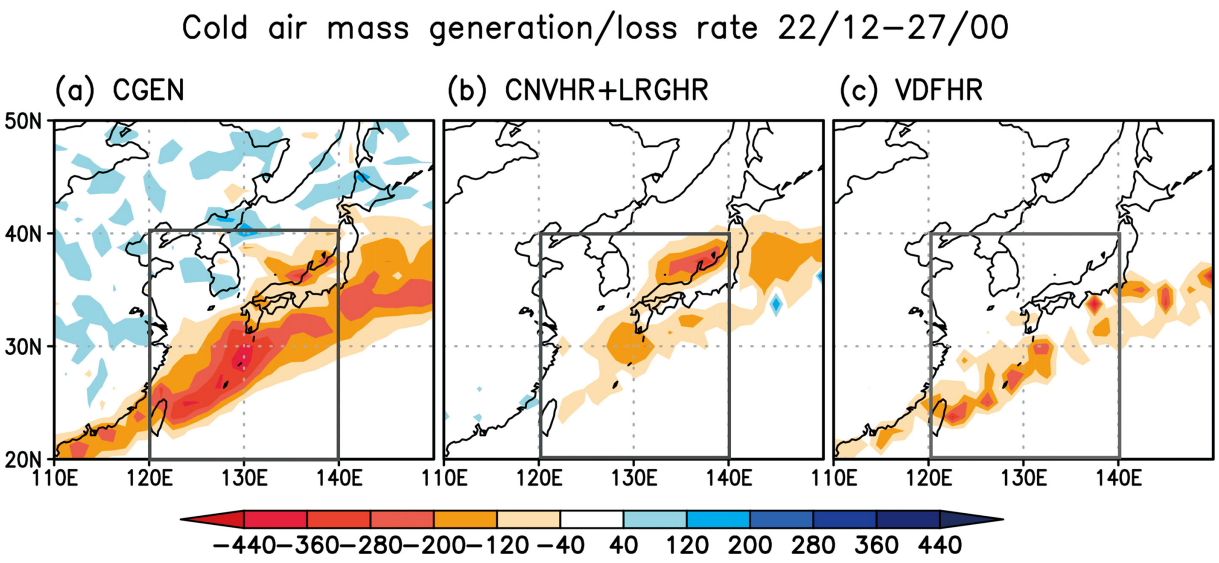

Fig. 6. Time average of (a) the total cold air mass generation/loss rate and its contribution from (b) the sum of convective and large-scale condensation heating and (c) vertical diffusion heating from 12UTC 22 January to 00UTC 27 January. The unit is hPa day^{-1}.

4.4 Evolution of negative heat content

Figure 7a shows the time evolution of the negative heat content and negative heat content flux. Overall, the thickness of the negative heat content shows a similar spatial pattern but at a larger change rate as against its maximum than that of the cold air mass during 16–24 January. During 16–20 January, the thick negative heat content grows to more than 9600 K hPa. It weakens rapidly during 22–24 January. Figure 7b presents the negative heat content generation rate caused by diabatic processes. The generation rate is largely positive and weak (about 1200 K hPa day^{-1}) when on the continent, and it becomes negative and quite strong (less than −6000 K hPa day^{-1}) when over the ocean surface. The thick negative heat content strengthens gradually when moving on the continent. It dissipates dramatically when touching the warm sea surface. The negative heat content loss region at 00UTC 24 January is broader than that of cold air mass loss region in Fig. 4c. As pointed out by I14, the diabatic change rate of the negative heat content is determined by diabatic processes of all layers below the 280 K isentrope, in contrast to that of cold air mass. Therefore, the surface diabatic processes strongly affect the loss rate of the negative heat content.

5. Abnormality of the event

The severe cold surge event of January 2016 is characterized by its extremely anomalous cold temperatures and consequent rare snowfall. To this point, the event has been characterized in terms of its dynamical features. Hereinafter, we assess the cold surge from another viewpoint: the abnormal nature of the cold surge.

The return periods of various metrics associated with the cold surge are presented in Fig. 8. Figure 8a shows that the return period of the cold air mass gets longer with the southward location from the southeast of Lake Baikal to southern China and north of the southwestern islands of Japan. The maximum return period becomes greater than 200 years at the southern edge of the cold air mass, especially over eastern China. The return period of the negative heat content shows a similar spatial pattern with that of the cold air mass, but we can see a northward extension of the longer return period (more than two years) in Fig. 8d. The longer return period of the cold air mass flux in Fig. 8b is also prominent south of 40°N, but it has a smaller region located at central Mongolia north of 40°N. In addition, as depicted in Fig. 8c, the region of the return period of more than two years in mean wind is confined to areas south of 40°N. The abnormal mean wind of once in 20 years or more is experienced mainly in central and southern China and also around Okinawa Island. The results described above suggest that the intensity of circulation becomes abnormal when the

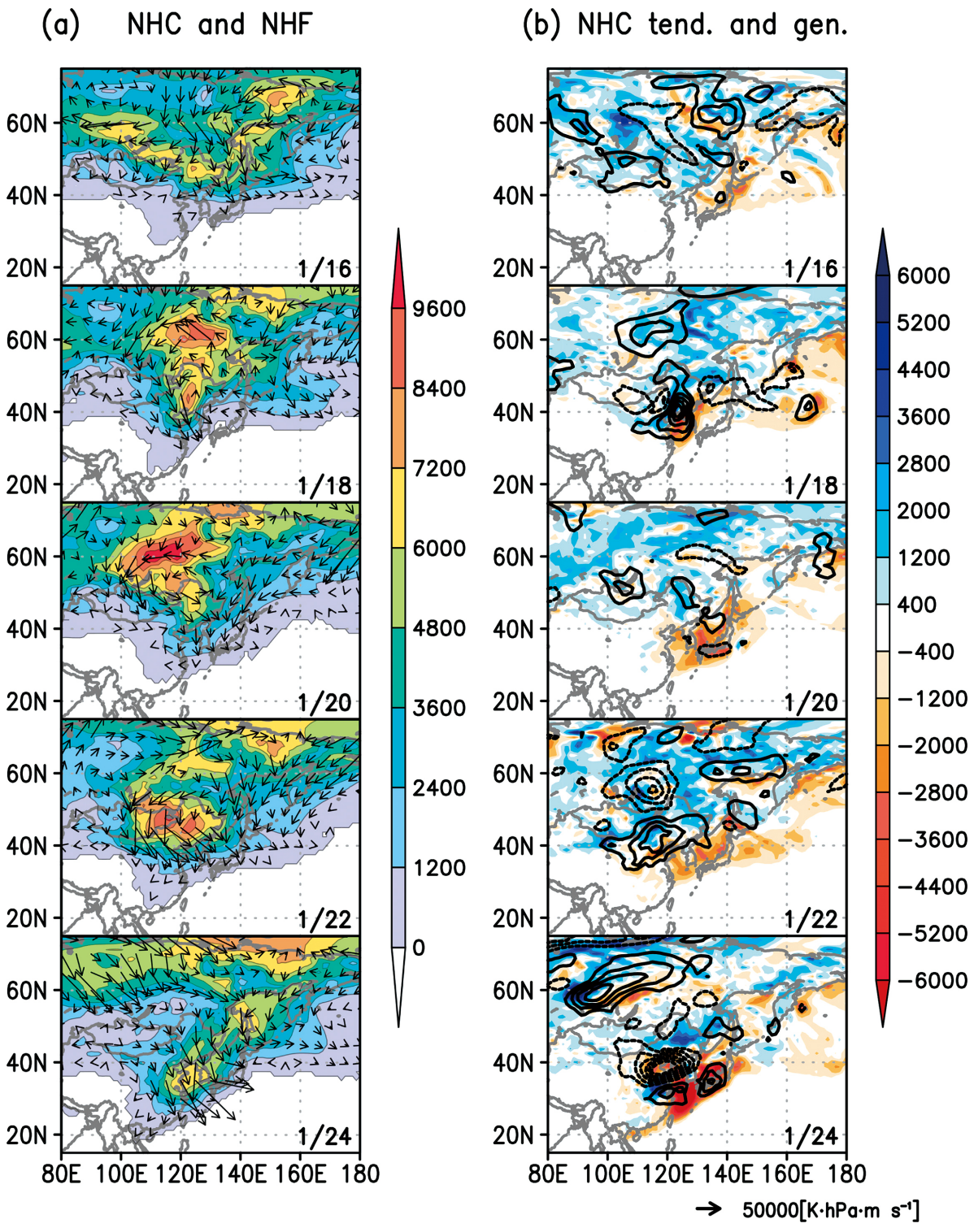

Fig. 7. (a) Negative heat content (K hPa; shaded) and negative heat content flux (K hPa m s^{-1}; arrows). (b) Negative heat content tendency (K hPa day^{-1}; contours) and negative heat content generation rate because of diabatic processes (K hPa day^{-1}; shaded) during 16–24 January 2016 at 00UTC. The contour interval in (b) is 1600 K hPa day^{-1}, and zero line is omitted. Dashed contours denote negative values.

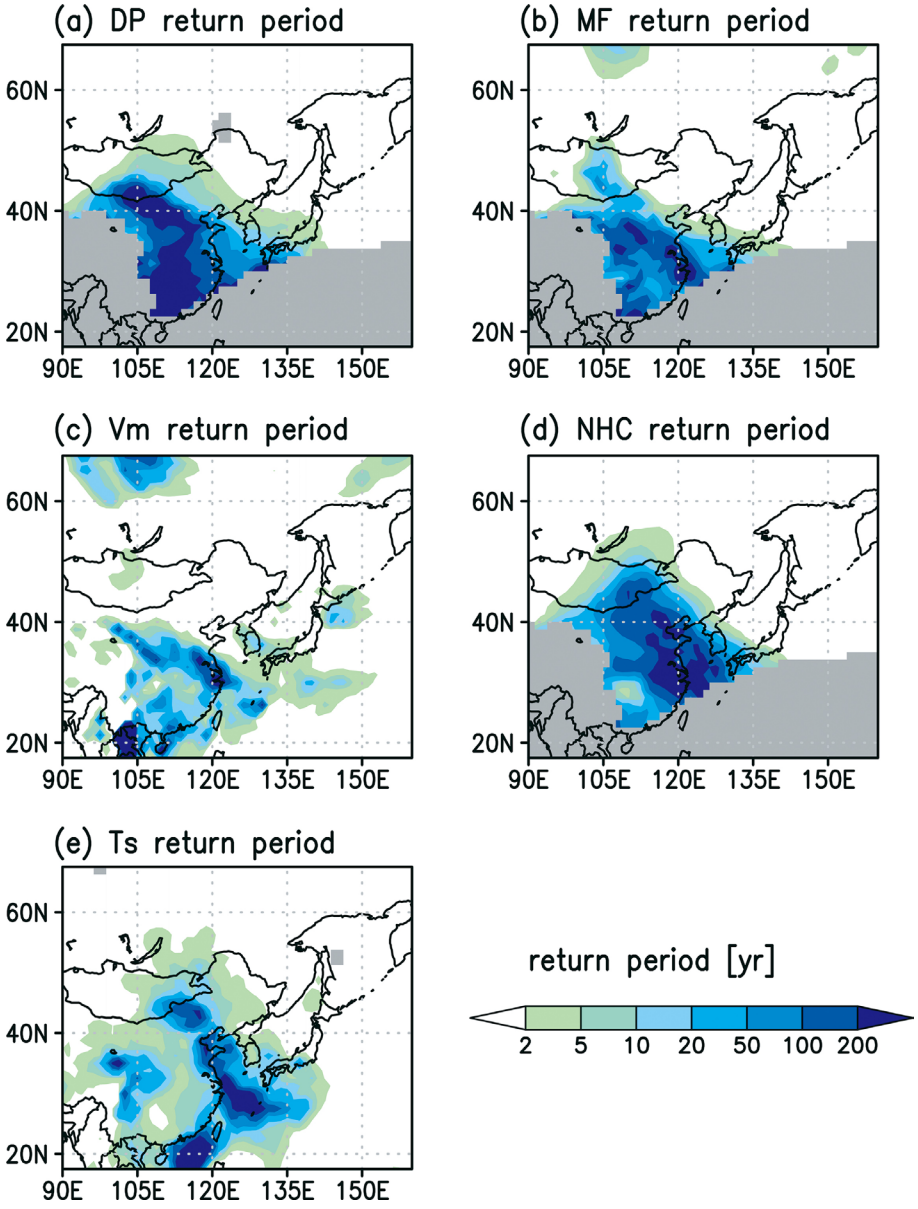

Fig. 8. Return period of the various metrics, including (a) cold air mass, (b) magnitude of cold air mass flux, (c) magnitude of mean wind, (d) negative heat content, and (e) surface temperature in this event (from 00UTC 14 January to 18UTC 25 January; the values of (a–d) are evaluated using maxima, (e) using minima in this event). The gray area shows the values that cannot be fitted with a GEV distribution (e.g., block maxima data including many zeros or iteration not converging).

cold air mass reaches areas south of 40°N, whereas the cold air mass has already become rare in terms of its thickness before crossing the 40°N parallel.

As depicted in Fig. 3, the cold air mass thickness near the center of the cold air mass shows a little change during its lifetime. However, the longer return period on the Sea of Okhotsk, Kolyma Lowland, and Central Siberia Plateau is not noticeable. This region has thick cold air masses in climatological mean. A large gradient of climatological mean cold air mass is

located near Lake Baikal (Shoji et al. 2014). Consequently, results suggest that the thick cold air masses "C1" and "C2" are not unusual, but migration of these cold air masses westward and southward makes the cold air mass thickness quite unusual. Considering the fact that the rarity of the cold air mass precedes that of the intensity of circulation, the southward migration of such a thick cold air mass is itself rather unusual. In other words, Fig. 8 suggests that it is a sufficiently rare event that such a thick cold air mass clump of Lake Baikal is swept southward thoroughly, even without considerable strength in terms of southerly impetus. Furthermore, in areas south of 40°N, southward migration of cold air mass occurs with strong southerly, which produces the CAO as an extreme cold surge for subtropical regions.

Figure 8e shows the return period of the surface temperature. A period longer than 100 years is seen mainly at the edge of the thick cold air mass, i.e., along the coast of eastern Asia, including the southern China and southwestern island of Japan. This is consistent with many reports of record-breaking temperatures and rare snowfall in this region, as referred in Section 1. Figures 8a, d show that the cold air mass and negative heat content are also record-breaking. Hence, Fig. 8 clarifies a characteristic of the cold surge event: the record-breaking cold surge event. As discussed above in this section, the record-breaking low temperatures over China and Japan are induced by the rare activities of cold air masses.

Comparing Fig. 8a with Fig. 8e, we notice that the cold air mass return period is clearer than that of surface temperature. This might be explained by the characteristics of the vertically integrated features of the cold air mass, i.e., the cold air mass also includes information of large-scale synoptic abnormal characteristics in the event. Of course, the definition of "intensity of extremeness" varies with the choice of variable. Figure 8e shows that the return period of surface temperature is consistent with our feeling of rarity. The return periods of cold air mass and its flux, as well as negative heat content, contain information related to the abnormality of the dynamical field in different aspects. Although a discussion about which definition is better is beyond the scope of our research, probably the abnormality of the isentropic cold air mass amount gives much information related to how the extreme weather occurs.

6. Discussion on dynamical behavior of tropospheric circulation associated with CAO

6.1 Possible relation between CAO and upper-level circulation in a view of tropopause potential temperature

Previous sections indicated a possible relation between the evolution of cold air mass and background circulation. Here, we further discuss this relation for a better understanding of the dynamical cause of the CAO event. To link cold air mass and CAO to large-scale circulation, we use the method presented by Hoskins and Berrisford (1988). They defined a 2-potential vorticity unit (PVU) surface as dynamical tropopause and considered potential temperature on the surface. With an adiabatic and frictionless motion, both potential temperature and potential vorticity are conserved following the motion in the Lagrangian sense. Therefore, the potential temperature on dynamical tropopause functions as a tracer. In addition, the distribution of potential temperature on dynamical tropopause can be connected with balanced circulation because of the invertibility principle of potential vorticity (e.g., Hoskins et al. 1985).

Figure 9 presents the potential temperature on dynamical tropopause. In climatology, the potential temperature is higher at lower latitudes and lower at higher latitudes, with equatorward potential temperature gradient. However, we can see the incursion of subtropical higher potential temperatures into the polar region in various places. An incursion of the high potential temperature into northern Siberia around 75°N, 115°E is one of these (marked with "H1"). The eastern and southern sides of the high potential temperature have lower potential temperatures below 300 K ("L1" and "L2"). On 18 January, "H1" on northern Siberia is cut off from the high potential temperature ridge and is then located on the 90°E parallel. At this time, "L1" and "L2" are southeastward of "H1." Comparison of Fig. 9 and Fig. 2 reveals that the location of the high potential temperature "H1" corresponds to the 500 hPa intense ridge R1 (Fig. 2b) and the surface SH (Fig. 2a): it may be the tropopause manifestation of the equivalent barotropic blocking ridge. Similarly, the low potential temperatures "L1" and "L2" on tropopause, respectively, correspond with the cutoff low "T1" and "T2" (c.f. Figs. 9, 2b). As explained by Pelly and Hoskins (2003), for instance, the cutoff high potential temperature may induce an anticyclone not only horizontally but also vertically and vice versa.

On 18 January, Fig. 9 shows another signal of massive scale leakage of high potential temperature

toward the north around the Caspian Sea on 50°E ("H2"). On 20 January, with close examination, one can see two high potential temperature regions around western Siberia. It represents that the potential temperatures "H1" and "H2" are merged. The time of merging nearly coincides with that of the onset of SH amplification, possibly implying the superposition of two induced lower circulations of "H1" and "H2". The quantitative degree of the resultant impact is calculated by Sato (2016). He found that the negative potential vorticity anomaly on western Siberia, which is the equivalent to the two high potential temperatures in our analysis, induces a positive height anomaly, which explains the +20 hPa amplification of the SH in the sea level pressure. On 22 January, the two anomalies "H1" and "H2" are already merged (and marked with "H"). The wave train of the potential temperature pattern is clear, with its axis orienting from south of the Scandinavian Peninsula to the Korean Peninsula.

Taking into account the analysis of circulation, we may explain the possible linkage between the daily behavior of cold air mass and the properties of tropopause potential temperature. On 16 January, the circulation induced by "H1", "L1", and "L2" represents northerly and northeasterly geostrophic winds from the bottom to the top of the troposphere over the region including the Kolyma Lowland, which results in the cold air mass flux from the Kolyma Lowland to the basin of southern Sakha. On 18 January, the dipole-like distribution of "H1" and "L1" over Siberia, with high potential temperature around the Kamchatka Peninsula, forms easterly geostrophic wind throughout the troposphere over northern Siberia (Fig. 2). As a result, a copious amount of cold air mass, mainly over the valley of southern Sakha, is washed away to Lake Baikal. After 20 January, the tropopause high and low potential temperature couplet of "H" and "L1" in the wave train may induce northerly geostrophic wind over the western part of the cold air mass. On the lower troposphere, there is also intensified SH accompanying strong pressure gradients. As a result, the induced circulation because of the upper and lower tropospheric anomalies causes a strong cold air mass flow southward. The quantitative analysis to prove the linkage between the CAO and tropopause circulation needs further analysis using, for example, the potential vorticity inversion method. It should be our future work.

6.2 *Some similarities and differences with typical CAO*

Comparing to the statistic CAOs by Shoji et al.

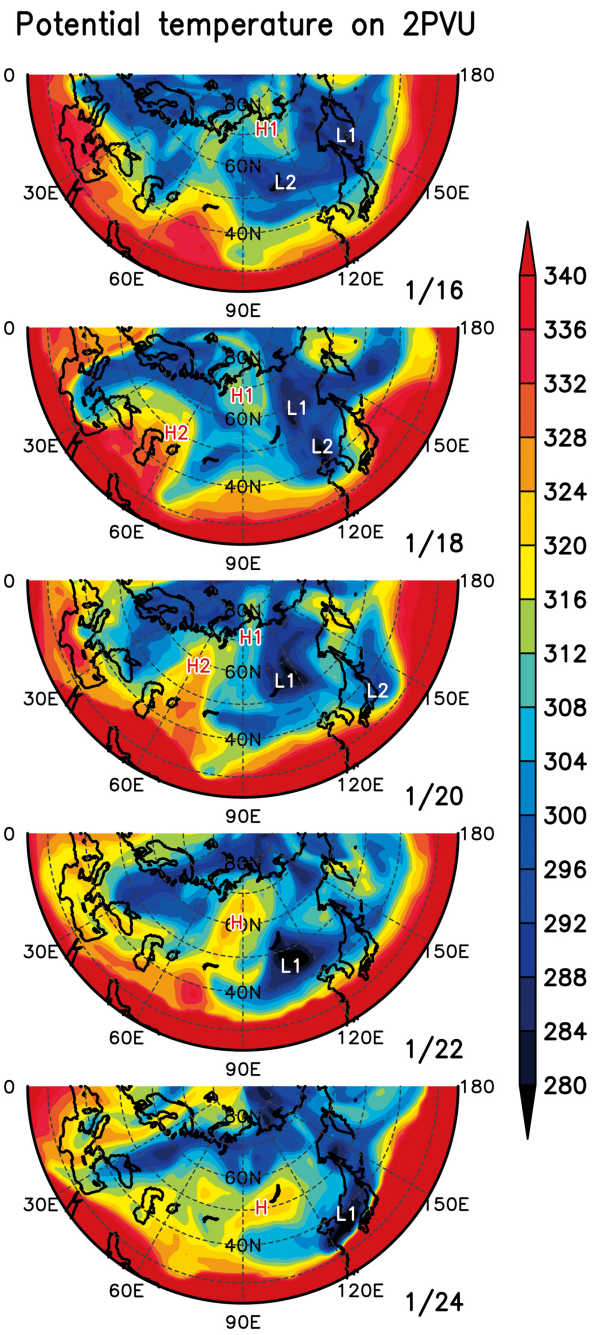

Fig. 9. Potential temperature (K; shaded) on the 2-PVU potential vorticity surface at 00UTC during 16–24 January 2016. Labels "H1", "H2", and "H" mark the regions of high potential temperature; "L1" and "L2" mark those of low potential temperature referred in the text.

(2014), our results show that this extreme cold surge event resembles the western CAO events of theirs. In western CAO, the cold air mass anomaly is accumulated from a wide variety of ranges of Siberia to Lake Baikal. Then, it proceeds to inland China. Finally, it decays by diabatic heating near the isotherm of 280 K SST line. These processes are similar to the cold surge event of January 2016. They also have many circulation features in common, including the southward propagating SH and short-lived synoptic-scale Okhotsk Low. In addition, earlier studies found that this strong CAO of January 2016 is related with upper-level wave-train-type circulation (Cheung et al. 2016; Song and Wu 2017), which is a well-known upper tropospheric circulation pattern associated with CAO (e.g., Takaya and Nakamura 2005a). However, as described in Section 5, this severe CAO of January 2016 is far from a typical CAO in terms of the intensity. Consequently, there must be something which makes the CAO quite unusual, and that is probably the feature before the beginning of the CAO. From our analysis, we identify that the thick cold air mass which causes the extreme cold surge migrates further from the Sea of Okhotsk and northeastern Siberia to the eastern side of SH. We also find the circulation pattern that blows the thick cold air mass westward, consisting of dipole pattern of blocking and cutoff low. These patterns resembles with the "Pacific-origin type" described by Takaya and Nakamura (2005b). The blocking over the arctic region of Siberia ("R1" in Fig. 2b), which characterizes the circulation pattern, should be necessary for accumulating thick cold air mass to Lake Baikal. It is eventually merged with the propagating ridge ("R2" in Fig. 2b). Therefore, this CAO of January 2016 may represent the result of the two circulation patterns that are favorable to the occurrence of CAO. They occur successively in a timely manner to produce the extreme CAO. We did not discuss the cause or rarity of the low pressure located on the east coast of Japan on 24 January. A possible connection may exist between the evolution of extratropical cyclone and the cold air mass of the Asian continent (Yoshida and Asuma 2004). The evolution of the low pressure associated with the CAO event remains an interesting topic that demands further investigation.

7. Conclusion

Using the isentropic method, we quantitatively analyzed the severe cold surge event that caused extremely low temperatures and rare snowfall over the mid-latitude and subtropical regions of East Asia on 24 January 2016. The processes associated with the evolution of the cold surge are presented schematically in Fig. 10. The results of our analyses suggest that the thick cold air mass "C" is built up over southern Sakha through cold air mass convergence caused by the northerly and northeasterly flow of cold air masses from the Kolyma Lowland "C2" and advection from the Sea of Okhotsk "C1". The thick cold air mass then migrates westward with easterly winds because of the dipole of the middle to upper-level blocking ridge and cutoff low. When the cold air mass reaches Lake Baikal, another ridge propagates from the Caspian Sea to the upstream of SH and intensifies it through superpositioning. The resultant middle to lower level meridionally oriented strong circulation then quickly guides the thick cold air mass southward. The southward flux of cold air mass is divided into two parts: one proceeds to the southwestern islands of Japan and Taiwan, and the other migrates along the lee slope of the Tibetan Plateau and reaches farther to Hong Kong. The cold air mass finally extinguishes over the ocean. On the whole, the time evolution of the thick cold air mass is dominated by adiabatic processes, especially advection by the mean wind of the cold air mass when it is moving over the continent. Diabatic generation by radiative cooling plays a secondary role in the intensification/maintenance of the cold air mass on the continent. In the cold air mass decay processes over the ocean, both adiabatic and diabatic processes play important roles. We found out that both vertical diffusion heating and precipitation-related heating equally contribute to the diabatic erosion of cold air mass. The analysis of quantifying the abnormality of the severe cold surge event using the extreme value theory was also performed. The abnormality of the cold air mass thickness increases considerably as the cold air mass migrates southward, although the thickness itself shows a slight change, which suggests that the normal thick cold air mass from the Sea of Okhotsk and northeastern Siberia becomes abnormal during westward and strong southward migration.

Using the quantitative value proposed by I14, the relation between CAO and large-scale circulation can be clarified in this extreme cold surge. The variables of the isentropic cold air mass analysis are conserved during migration. Therefore, we succeeded in tracking the clump of cold air mass more than one week ahead of the outbreak of cold air to subtropical East Asia with dynamic consistency. Moreover, we found out that this analysis method is suitable for investigating the evolution processes of cold air mass. Equation (5) divides the factor of cold air mass evolution into

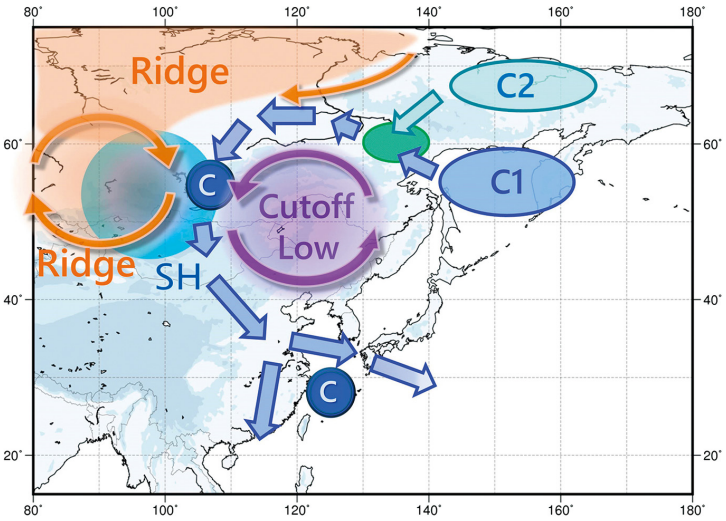

Fig. 10. Schematic diagram showing the evolution of the extreme cold surge event on January 2016. The blue circle with white text "C" marks the center of the cold air mass clump. Dark blue arrows indicate the propagation route. The light blue circle with text "C2" represents a cold air mass over the Kolyma Lowland on 16 January. The dark blue circle with text "C1" signifies a cold air mass over the northern Sea of Okhotsk on the same day. The light blue arrow shows northeasterly on 16 January. The green hatched circle shows the cold air mass convergence area on the same day. The area painted orange shows 500 hPa ridges: one north of 60°N is a ridge in the arctic region of Siberia during 16–18 January; the other is a propagating ridge on 22 January. Orange arrows indicate 500 hPa wind related with the ridges. The circle painted purple shows the cutoff low at 500 hPa on 22 January. Purple arrows indicate 500 hPa wind related with the cutoff low. The circle painted blue marks the area around the center of the Siberian High on that day. On the background map, the areas shaded light and deep blue, respectively, show areas above 750 and 1500 m in geographical height.

three parts, with the roles of respective factors differing from each other on the continent and over the ocean. In addition, the cold air mass and negative heat content of this analysis method show clear signals for quantifying the rarity of the extreme event from its integrated features: small-scale or thin-layer abnormal coldness is filtered out; large-scale cold events are emphasized. The region of long return period is noticeable in this case of extreme cold. In summary, this study of the extreme cold surge that occurred in East Asia in January 2016 shows that the isentropic cold air mass analysis method has potential for describing extreme cold surges clearly and quantitatively.

Cold surges are associated with extreme weather conditions in the winter season. The variations of extreme CAO occurrences in the warming climate have a significant implication for disaster prevention and mitigation. In past decades, the extreme low-temperature events have decreased dramatically over China, with a close relation to the global warming. Many studies also indicated a weakening of EAWM that may contribute to decreasing events of low temperature (e.g., Wang and Chen 2014). Although cold air masses at high latitudes may decrease (Kanno et al. 2016), the analysis of this study indicates that strong cold surges are still possible with anomalous strong southward movement guided by active wave trains. The deepening of low pressure over the warm moist ocean surface may also play a role. During the winter of 2016, owing to the extreme cold surge events, 919 site-days of extreme low temperature were observed over mainland China, which were much more than the climate mean since 1961 (approximately 520 site-days) and those in the last 10 years (approximately 200 site-days). These significant features urge more analysis of CAO activities, especially those associated with extreme cold surge events in the changing climate. The quantitative analysis based on the isentropic method may provide more details on the East Asian climate from the perspective of cold air masses. Further studies are warranted to provide more insight into the evolution of cold surge events and their long-term variations as well as the resultant extreme weather.

Acknowledgment

We thank two anonymous reviewers to improving the quality of the paper. The JRA-55 reanalysis dataset is provided by Japan Meteorological Agency (JMA) and downloaded from JMA Data Distribution System (ftp://ds.data.jma.go.jp). This work was supported in part by JSPS KAKENHI Grant Number JP15H02129, the Social Implementation Program on Climate Change Adaptation Technology (SI-CAT), and the National Key Research and Development Program of China (Grant number 2016YFA0600704).

References

Abdillah, M. R., Y. Kanno, and T. Iwasaki, 2017: Tropical–extratropical interactions associated with East Asian cold air outbreaks. Part I: Interannual variability. *J. Climate*, **30**, 2989–3007.

Boville, B. A., 1985: The thermal balance of the NCAR community climate model. *J. Atmos. Sci.*, **42**, 695–709.

Chang, C.-P., J. E. Millard, and G. T. J. Chen, 1983: Gravitational character of cold surges during winter MONEX. *Mon. Wea. Rev.*, **111**, 293–307.

Chang, C.-P., Z. Wang, and H. Hendon, 2006: The Asian winter monsoon. *The Asian Monsoon*. B. Wang (ed.), Praxis Publishing, UK, 89–127.

Cheung, H. N., W. Zhou, Y. Shao, W. Chen, H. Y. Mok, and M. C. Wu, 2013: Observational climatology and characteristics of wintertime atmospheric blocking over Ural-Siberia. *Climate Dyn.*, **41**, 63–79.

Cheung, H. H. N., W. Zhou, M. Y. T. Leung, C. M. Shun, S. M. Lee, and H. W. Tong, 2016: A strong phase reversal of the Arctic Oscillation in midwinter 2015/2016: Role of the stratospheric polar vortex and tropospheric blocking. *J. Geophys. Res.*, **121**, 13443–13457.

Ding, Y., 1990: Build-up, air mass transformation and propagation of Siberian high and its relations to cold surge in East Asia. *Meteor. Atmos. Phys.*, **44**, 281–292.

Ding, Y., and T. N. Krishnamurti, 1987: Heat budget of the Siberian high and the winter monsoon. *Mon. Wea. Rev.*, **115**, 2428–2449.

Ding, Y., and D. R. Sikka, 2006: Synoptic systems and weather. *The Asian Monsoon*. B. Wang (ed.), Praxis Publishing, UK, 131–201.

Hoskins, B., and P. Berrisford, 1988: A potential vorticity perspective of the storm of 15–16 October 1987. *Weather*, **43**, 122–129.

Hoskins, B. J., M. E. McIntyre, and A. W. Robertson, 1985: On the use and significance of isentropic potential vorticity maps. *Quart. J. Roy. Meteor. Soc.*, **111**, 877–946.

Iwasaki, T., T. Shoji, Y. Kanno, M. Sawada, M. Ujiie, and K. Takaya, 2014: Isentropic analysis of polar cold airmass streams in the Northern Hemispheric winter. *J. Atmos. Sci.*, **71**, 2230–2243.

Joung, C. H., and M. H. Hitchman, 1982: On the role of successive downstream development in East Asian polar air outbreaks. *Mon. Wea. Rev.*, **110**, 1224–1237.

Kanno, Y., M. R. Abdillah, and T. Iwasaki, 2015: Charge and discharge of polar cold air mass in Northern Hemispheric winter. *Geophys. Res. Lett.*, **42**, 7187–7193.

Kanno, Y., M. R. Abdillah, and T. Iwasaki, 2016: Long-term trend of cold air mass amount below a designated potential temperature in Northern and Southern Hemispheric winters using reanalysis data sets. *J. Geophys. Res.*, **121**, 10138–10152.

Kobayashi, S., Y. Ota, Y. Harada, A. Ebita, M. Moriya, H. Onoda, K. Onogi, H. Kamahori, C. Kobayashi, H. Endo, K. Miyaoka, and K. Takahashi, 2015: The JRA-55 Reanalysis: General specifications and basic characteristics. *J. Meteor. Soc. Japan*, **93**, 5–48.

National Climate Center, 2017: *China Climate Bulletin (2016)*. Science press, Beijing, 100 pp (in Chinese).

Oikawa, Y., and K. Kamiguchi, 2016: Summary of the 2015/2016 Asian winter monsoon. *TCC News*, **44**, 6–13.

Papritz, L., and S. Pfahl, 2016: Importance of latent heating in mesocyclones for the decay of cold air outbreaks: A numerical process study from the Pacific sector of the Southern Ocean. *Mon. Wea. Rev.*, **144**, 315–336.

Park, T.-W., C.-H. Ho, and Y. Deng, 2014: A synoptic and dynamical characterization of wave-train and blocking cold surge over East Asia. *Climate Dyn.*, **43**, 753–770.

Pelly, J. L., and B. J. Hoskins, 2003: A new perspective on blocking. *J. Atmos. Sci.*, **60**, 743–755.

Sato, H., 2016: 2015/16 winter monsoons in East Asia. *12th FOCRAII*, Guangzhou, China. [Available at http://ds.data.jma.go.jp/gmd/tcc/tcc/library/FOCRAII_1604/2015-16_winter_monsoon.pdf.]

Shoji, T., Y. Kanno, T. Iwasaki, and K. Takaya, 2014: An isentropic analysis of the temporal evolution of East Asian cold air outbreaks. *J. Climate*, **27**, 9337–9348.

Song, L., and R. Wu, 2017: Processes for occurrence of strong cold events over eastern China. *J. Climate*, **30**, 9247–9266.

Stephenson, A. G., 2018: *Package* '*ismev*'. [Available at https://cran.r-project.org/web/packages/ismev/ismev.pdf.]

Takahashi, R., and T. Shimura, 2016: *Extreme Value Statistics*. ISM series: Evolving statistical mathematics, Kindai Kagaku Sha, 262 pp (in Japanese).

Takaya, K., and H. Nakamura, 2005a: Mechanisms of intraseasonal amplification of the cold Siberian high. *J. Atmos. Sci.*, **62**, 4423–4440.

Takaya, K., and H. Nakamura, 2005b: Geographical dependence of upper-level blocking formation associated with intraseasonal amplification of the Siberian high. *J. Atmos. Sci.*, **62**, 4441–4449.

Wallace, J. M., and D. S. Gutzler, 1981: Teleconnections in the geopotential height field during the Northern Hemisphere winter. *Mon. Wea. Rev.*, **109**, 784–812.

Wang, L., and W. Chen, 2014: An intensity index for the East Asian winter monsoon. *J. Climate*, **27**, 2361–2374.

Wang, L., and M.-M. Lu, 2016: The East Asian Winter Monsoon. *The Global Monsoon System: Research and Forecast. 3rd Edition*. Chang, C.-P., H.-C. Kuo, N.-C. Lau, R. H. Johnson, B. Wang, and M. C. Wheeler (eds.), World Scientific Publishing, UK, 51–61.

Wang, L., W. Chen, W. Zhou, J. C. L. Chan, D. Barriopedro, and R. Huang, 2010: Effect of the climate shift around mid 1970s on the relationship between wintertime Ural blocking circulation and East Asian climate. *Int. J. Climatol.*, **30**, 153–158.

Yoshida, A., and Y. Asuma, 2004: Structures and environment of explosively developing extratropical cyclones in the northwestern Pacific region. *Mon. Wea. Rev.*, **132**, 1121–1142.

Zhang, Y., K. R. Sperber, and J. S. Boyle, 1997: Climatology and interannual variation of the East Asian winter monsoon: Results from the 1979–95 NCEP/NCAR Reanalysis. *Mon. Wea. Rev.*, **125**, 2605–2619.